LA-UR 95-0371

TITLE: PARTICULATE SIZE DISTRIBUTIONS AND SEQUENTIAL FRAGMENTATION/TRANSPORT THEORY

AUTHOR(S): Kenneth Wohletz (EES-1) and Wilbur Brown (5179 Eastshore Drive, Lake Almanor, CA 96137)

Los Alamos

Los Alamos National Laboratory
Los Alamos, New Mexico 87545

PARTICULATE SIZE DISTRIBUTIONS AND
SEQUENTIAL FRAGMENTATION/TRANSPORT THEORY

Kenneth Wohletz
Los Alamos National Laboratory
EES-1, MS D462
Los Alamos, NM 87545
(505)667-9202

Wilbur Brown
5179 Eastshore Drive
Lake Almanor, CA 96137
(916)284-7590

ABSTRACT

Particulate size distributions offer the scientist important clues about the mechanism(s) responsible for their formation. These distributions are complex, often being the combination of several subpopulations that bear the signature of specific fragmentation and particulate transport processes. Historically, such distributions have been characterized by some empirical distribution law such as the lognormal or Weibull distributions, but such characterizations provide little insight into sample origins. We have developed a sequential fragmentation/transport theory (SFT) that predicts particulate mass/size distributions, based on idea that fragmentation and transport mechanisms operate in a sequential fashion, breaking up a parental mass into ever smaller ensembles of daughter particles and then sorting them according to mass. Integration of the results of each step in a given sequence predicts a distribution bearing resemblance to the lognormal and Weibull distributions. The free parameter for fragmentation (γ) and its analog for transport (τ) describe the mass sensitivity for solutions to Navier-Stokes equations. In this fashion, distributions can be predicted for a certain fragmentation and transport mechanism, and by inverse law, these mechanisms may be constrained by measurement of size data. In describing SFT, we show its application to experimental debris from thermite/water explosions and volcanic eruptions in which the thermodynamic efficiency of water/melt interaction is directly related to γ. Our conclusion based on preliminary application of SFT is that intense multiphase vapor explosions involve fragmentation/propagation mechanisms whose character is dependent on the mass ratio of water and melt interacting.

I. INTRODUCTION

From the perspective of a volcanologist, one of the most distinguishing features of *hydrovolcanic* explosions (those caused by interaction of hot magma with water) is the very fine-grained character of ejected materials (called *tephra*). Hydrovolcanic tephra are composed of quenched magma fragments and pieces of rock excavated during crater formation, and in many cases, the average diameters of these tephra are several tens of micrometers. This size range can be contrasted to tephra from *magmatic* explosions (those cause by rapid decompression of a volatile charged magma), which commonly show average diameters from several hundreds of micrometers to several millimeters. This general observation has led numerous researchers to do extensive size-distribution analyses of hydrovolcanic tephra to better understand the mechanisms involved in melt fragmentation. The main problem with this work is that particulate size distribution analysis has traditionally been an empirical process, limited to statistical treatment based on assumptions of various distribution laws such as the lognormal, Weibull, Rosin-Rammler, and more recently fractal.

In this paper, We discuss the development of the sequential fragmentation/transport theory (SFT) for particulate analyses and will attempt to show how its basis in physical theory allows size data inversion to constrain fragmentation mechanisms.

II. SEQUENTIAL FRAGMENTATION/TRANSPORT

A fundamental observation of fragmentation processes is that they generally follow a sequence of events involving crack nucleation, growth, and branching, during repetitive material stress and strain. For example during brittle failure, stress waves and their reflections propagate through a material many times during their decay, or in the case of hydrodynamic fragmentation, repeated growth and detachment of surface instabilities take place. This observation has led us to model fragmentation as an integral process in which a parental mass produces an ensemble of daughter fragments of various sizes, each daughter fragment then repeatedly becoming the parent for further daughter ensembles (Fig. 1). Conserving total mass, this integral formulation is

$$n(m) = c \int_m^\infty n(m') f(m' \to m) dm' \quad , \quad (1)$$

where $n(m)$ is the number distribution in units of particles per unit mass of mass m between m and $m + dm$, c is constant, $n(m')$ is the number distribution of parental mass m', and $f(m' \to m)$ is the single-event particle distribution function and expresses the distribution in mass, m, arising from the fragmentation of a single, more massive particle of mass m'. In this fashion, Equation (1) represents the summing of all contributions to the distribution of m from the fragmentation of all particles of mass $m' > m$.

To solve Equation (1) we have assumed that fragmentation mechanisms are mass sensitive; in other words that solutions to fragmentation mechanisms will always show a mass dependency. We have chosen to express this mass dependency as a power law from consideration of previous theoretical work.[1] Brown[2] set the constant $c = m^{-1}$ such that the transfer function is

$$f(m' \to m) = \left(\frac{m}{m_1} \right)^\gamma \quad . \quad (2)$$

Here, m_1 denotes a mass related to the average distribution mass and γ is a free parameter where $-1 > \gamma \le 0$. Inserting Equation (2) into Equation (1), we have

$$n(m) = \left(\frac{m}{m_1} \right)^\gamma \int_m^\infty n(m') \, d\left(\frac{m'}{m_1} \right) \quad . \quad (3)$$

The solution to Equation (3) is

$$n(m) = \frac{N_T}{m_1} \left(\frac{m}{m_1} \right)^\gamma \exp\left[-\frac{\left(\frac{m}{m_1} \right)^{\gamma+1}}{\gamma+1} \right] \quad , \quad (4)$$

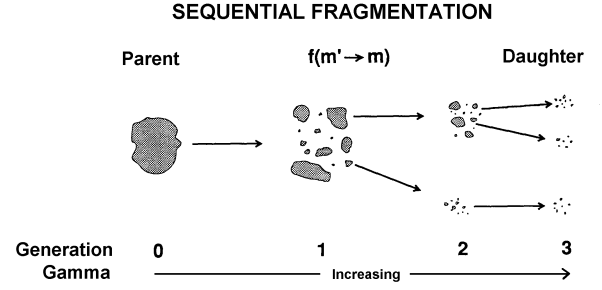where Equation (4) has been normalized to the total number of fragments N_T:

Figure 1. Schematic illustration of sequential fragmentation.

$$N_T = \int_0^\infty n(m) dm \quad . \quad (5)$$

Brown and Wohletz[3] have shown Equation (4) to be the Weibull[4] distribution in particle number.

Equation (4) is a distribution with some basic relationships. The free parameter γ models the *maturity* of the fragmentation process. Where γ is close to -1, SFT models *sudden* fragmentation processes that involve only one or a few stages of breakage, such as the passage of a single compression/rarefaction stress pair leading to fragmentation, a situation that creates a broad, poorly defined distribution of fragment sizes. As γ increases, SFT models fragmentation processes that represent the culmination of many individual breakage events, such as the repeated growth and detachment of instabilities at a fragment surface; with increasing γ the resulting distribution has a much greater central tendency (lower dispersion) and finer average size. Furthermore, Brown and Wohletz[3] have shown that through the form of Equation (2), Equation (4) is fractal with 3γ being the fractal dimension.[5] In addition, by dividing Equation (4) by Equation (5), one obtains a cumulative distribution of the Rosin-Rammler[6] form in particle number.

Because particle size data is often measured as the mass of particles in a bins of fixed size ratio, we can express Equation (4) as a mass distribution, $mn(m)$:

$$mn(m) = N_T \left(\frac{m}{m_1} \right)^{\gamma+1} \exp\left[-\frac{\left(\frac{m}{m_1} \right)^{\gamma+1}}{\gamma+1} \right] \quad . \quad (6)$$

Alternatively, if we make use of a logarithmic scale in m, say $u \equiv \ln m$, noting that $n(u)du = n(m)dm$, then $mn(m) = n(u)$ Thus $mn(n)$ also gives the number of particles per unit natural logarithm in m. Furthermore, if $mn(m)$ is the number of particles per unit logarithm in m, and the mass of each particle is m, then the total mass of particles per unit logarithm is just $m^2 n(m)$. Thus

$$m^2 n(m) = N_T m_1 \left(\frac{m}{m_1}\right)^{\gamma+2} \exp\left[-\frac{\left(m/m_1\right)^{\gamma+1}}{\gamma+1}\right] \quad . \quad (7)$$

This distribution is shown in Figure 2 where it is compared to the lognormal distribution:

$$\lambda(m) = \frac{1}{\sigma\sqrt{2\pi}} \exp\left[-\frac{\left(\ln m - \ln m_3\right)^2}{2\sigma^2}\right] \quad , \quad (8)$$

where $\lambda(m)$ is the mass, m, distribution in units of mass per unit ln interval, m_3 is a constant that allows variable positioning of the curve, and σ is the standard deviation in $\ln m$ units.

The quantity $m^2 n(m)$ is precisely what is measured when a sample of particles is sifted through a series of sieves of decreasing mesh size where the mesh sizes between any two adjacent sieves is a fixed ratio. As Brown and collaborators noted[1,7], the form $m^2 n(m)$ closely resembles the lognormal distribution[8] (see Fig. 2), a distribution that has enjoyed a long history of successful, empirical use; we note the lognormal distribution has a mathematical basis[9], but no physical basis.

The gathering of data through a series of sieves with a fixed size ratio between them is standard procedure in many fields; for example, in the analysis of geological materials such as sand and volcanic ash. For this procedure, the mass left on each sieve ΔM, is recorded in a logarithmic bin of width $\Delta\phi$ where $\phi \equiv -\log_2(\ell/\ell_0)$, and where $\ell_0 \equiv 1$ mm. It can easily be shown that

$$\frac{dM}{d\phi} = -3\ln 2 \; m^2 n(m) \quad . \quad (9)$$

The negative sign and the ln 2 originate from the definition of the ϕ-scale, and the 3 provides the conversion from mass to size (assuming spherical particles of equal density). An illustration of the effect of varying γ in Equation (7) is shown by Figure 3 where distributions of different γ values are plotted as $dM/d\phi$ vs ϕ from Equation (9). This illustration shows that as γ increases (signifying that the particles are undergoing further processing), the distribution becomes finer in particle size and more *peaked*.

As in many fields, the lognormal distribution has been typically used to describe the data because it is a convenient approximation to the shape of the data such as $dM/d\phi$. Although application of the lognormal distribution to this type of data is traditional, its satisfactory representation of the data may be simply fortuitous. In contrast, we believe that application of Equation (18), giving $m^2 n(m)$, is a more proper, physically based formulation to apply. An example of the use of $m^2 n(m)$ for soot particle size data[10], using the mass to size conversion of Equation (20), is shown in Figure 4.
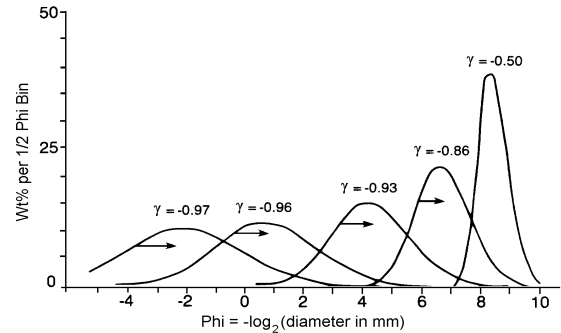
Figure 3. Plot of $m^2 n(m)$ distributions in the form of $dM/d\phi$ vs ϕ, where $dM/d\phi$ is defined by Equation (20), and $\phi = -\log_2$(diameter in mm); the reader will recall that all log scales are proportional, and that the minus sign simply places the coarse particles to the left and the fine particles to the right. This plot shows the effect of varying γ in Equation (18), where increasing γ shifts the peak of the distribution to the right (finer particle sizes) and makes the distribution more peaked. Note that where $\gamma = -1.0$ the distribution is flat.
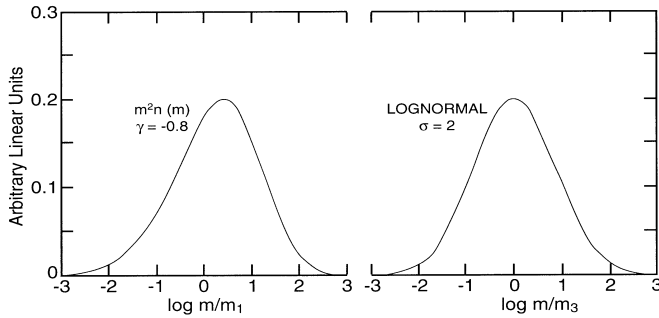
Figure 2. Plot of Equation (7) expressing $m^2 n(m)$ vs log m compared to lognormal curve [Equation (8)]. The standard deviation $\sigma=2$ for the lognormal curve closely matches $\gamma=-0.8$ for the sequential fragmentation curve (m_1 and m_3 are constants related to the average mass of each distribution).

$$p(\xi)dx = \frac{dx}{\xi} \qquad (11)$$

where ξ is the range of a particle related to its mass by

$$\xi = \xi_o\left(\frac{m}{m_2}\right)^{-\tau} . \qquad (12)$$

SEQUENTIAL TRANSPORT

Figure 5. Schematic illustration of sequential transport.

The free parameter τ is analogous to γ is Equation (2) and represents the mass dependency of the transport mechanism (*e.g.* ballistic, suspended, saltating, tractive). Equation (10) has the solution[7] in the range of x and m of interest of

$$m^2n(x,m) \cong K\left(\frac{m}{m_2}\right)^2 \exp\left[-\left(\frac{x}{\xi_o}\right)\frac{\left(m/m_2\right)^{\tau+1}}{\tau+1}\right] , \qquad (13)$$

similar to Equation (7) where K is a normalizing constant. With size frequency data reported by the ϕ-scale, Equation (13) becomes

$$\frac{dM}{d\phi} = K_2\ell^6 \exp\left[-\frac{x}{\xi_o}\frac{\ell^{3(\tau+1)}}{\tau+1}\right] . \qquad (14)$$

In Equation (14), K_2 is unity for size-frequency histogram data and x/ξ_o as justified by Wohletz *et al.*[7]

Because fragments sampled from explosions have varying shapes and density, the assumption of constant density and spherical shape makes the solution given in Equation (14) of limited practicality. Wohletz *et al.*[7] show that conversion particle diameters to masses follows

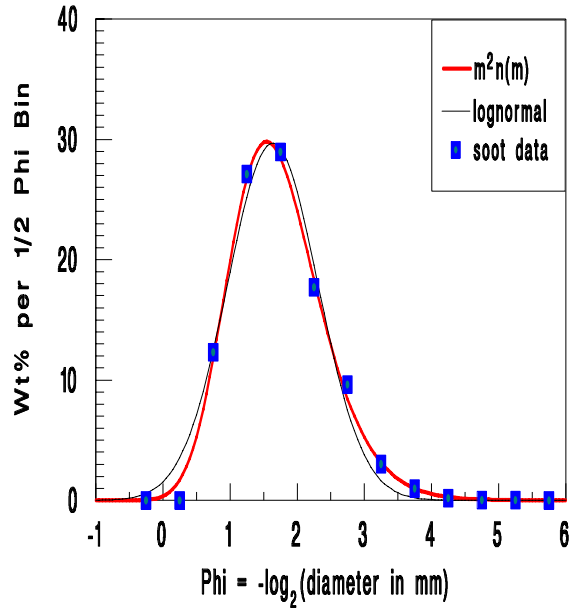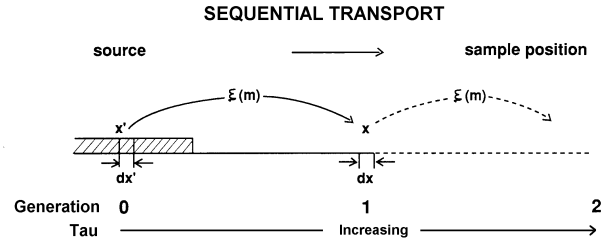$$m = \frac{4}{3}\pi S\rho\left(\frac{\ell}{2}\right)^3 , \qquad (15)$$

Figure 4. An example of the use of $m^2n(m)$ for soot particle data from Medalia and Heckman[10]. In this plot the $m^2n(m)$ curve crosses every data point but one, whereas the lognormal curve gives a less satisfactory fit. Each curve was best-fit to data by least-squares regression analysis; the $m^2n(m)$ curve explains 96% of the sample variance while the lognormal curve satisfies only 88%. As in Figure 4, data and $m^2n(m)$ are expressed in distribution wt% per 1/2 phi bins.

A fundamental sampling problem inherent in volcanological studies is that it is difficult if not impossible to obtain a sample that has not been modified by a transporting agent. In this light, the sample size distribution reflects as much, and in many cases, more processing by transport than by explosive fragmentation. Transport not only sorts particles by size via gravitational and drag forces, it can cause particle collisions that further cominute the sample. Wohletz *et al.*[7] analyzed this problem by again considering transport effects as a sequential process (Fig. 5) as in Equation (1):

$$n(x,m) = c_2\int_0^m\int_{x-\xi}^0 n(x',m)p(\xi)dx'dm' . \qquad (10)$$

In this equation, $n(x,m)$ is the particle number distribution in the length interval between x and $x+dx$ and mass interval between m and $m+dm$. The function $p(\xi)$ is the probability that a particle transported from the source x' will be sampled at position x:

where S is a shape factor typically defined as $S = P^2/(4\pi A)$ for which P is the particle perimeter and A is its area. Differentiating the logarithm of Equation (15), we find that Equation (9) becomes

$$\frac{dM}{d\phi} = -m^2 n(x,m)\left[3\ln 2 + \frac{dS}{S d\phi} + \frac{d\rho}{\rho d\phi}\right] \quad , \quad (16)$$

such that Equation (14) becomes

$$\frac{dM}{d\phi} = K_3 \ell^6 \exp\left[-\frac{\ell^{3(\tau+1)}}{\tau+1}\right]$$
$$+ K_S \ell^6 \exp\left[-\frac{\ell^{3(\tau_S+1)}}{\tau_S+1}\right] \quad , \quad (17)$$
$$+ K_\rho \ell^6 \exp\left[-\frac{\ell^{3(\tau_\rho+1)}}{\tau_\rho+1}\right]$$

which predicts that the size-frequency distribution of a sample composed of fragments of varying shape and density will be the sum of at least three subpopulations showing K_3, K_S, and K_ρ fraction of the total with SFT free parameters τ, τ_S, and τ_ρ respectively.

III. Application of SFT to Particulates Sampled from Intense Multiphase Interactions

We have investigated samples from a broad range of fragmentation processes including the stellar initial mass function, galactic luminosities, asteroids, infalling extraterrestrial material (meteoritic), iron ground in a ball mill, high explosive aerosolization, water/thermite explosions, fly ash from coal-fired and wood-burning generating plants, and geologic samples (windblown dust, water-laid sands, and volcanic ash). Many of these examples have been documented by Brown[2], but it is those samples from water/thermite explosions[11,12] and volcanic eruptions[13] that are of greatest interest for this forum. In analysis of these samples, we note that few, if any, represent distributions unaltered by transport processes, such that application of SFT by the form given in Equation (17), requires considerations of both the effects of fragmentation and transport on SFT free parameters.

As a first example, we explore samples taken from thermite/water volcanic analog experiments.[11,12] Due to the fact that these experiments involved a range of mechanical designs, only several can be compared as having similar

sample bias. In Figures 5, we show size frequency distributions for three similar experiments. Note that 6 subpopulations are identified in each experimental sample with individual subpopulations showing similar distribution parameters in each sample. These subpopulations derive from variations in particle bulk density and shape, which can be related to the interplay of several fragmentation mechanisms. For each of these experiments, Figure 6 shows the average fragmentation parameter (γ) bearing a direct relationship to the observed mechanical conversion ratio[12] (expressed as the percentage of initial thermal energy converted to mechanical energy measured). This relationship shows γ increasing linearly with conversion ratio, meaning that experiments producing greater measurable explosive energy involve a fragmentation mechanism that is more highly evolved. Wohletz *et al.*[7] predicted this behavior based on theoretical relationships among fragment mass, surface areas, and resulting heat transfer rates. Brittle fragmentation (thermal shattering) of glassy substances results in lower γ values and surface area per unit mass and heat transfer rates than do hydrodynamic (ductile) deformation processes; hence an expected increase in γ with explosive efficiency. A more detailed discussion of hydrovolcanic fragmentation mechanisms is given by Wohletz[14], based on considerations of fragment size and shape.
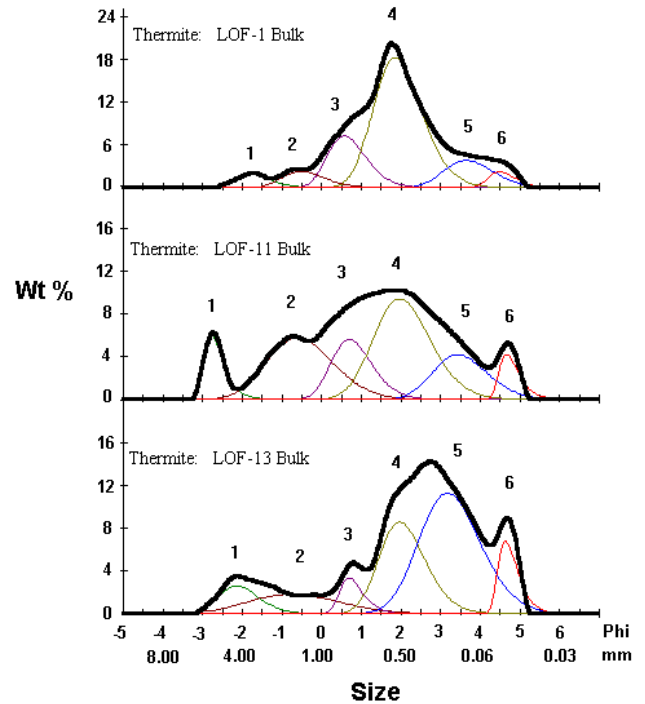

Figure 5. Size-frequency plots of three bulk samples from thermite/water volcano experiments.[12] Total distributions are shown in bold curves and subpopulations in thin curves. The subpopulation parameters of mode, dispersion (γ), and fraction for samples LOF-1, LOF-11, and LOF-13 are respectively: **Subpopulation 1:** -1.82, -2.79, -2.15 (mode), -0.40, 1.00, -0.52 (dispersion), and 0.04, 0.08, 0.07 (fraction); **Subpopulation 2:** -0.51, -0.60, -0.76 (mode), -0.59, -0.83, -0.91 (dispersion), and 0.06, 0.24,

0.11 (fraction); **Subpopulation 3:** 0.58, -0.70, 0.69 (mode), -0.50, -0.55, 0.42 (dispersion), and 0.18, 0.15, 0.05 (fraction); **Subpopulation 4:** 1.86, 1.97, 1.97 (mode), -0.68, -0.77, -0.65 (dispersion), and 0.56, 0.34, 0.25 (fraction); **Subpopulation 5:** 3.65, 3.43, 3.17 (mode), -0.70, -0.75, -0.80 (dispersion), and 0.12, 0.14, 0.447 (fraction); **Subpopulation 6:** 4.49, 4.67, 4.64 (mode), 0.04, 0.05, 0.09 (dispersion), and 0.04, 0.05, 0.09 (fraction). Note mode sizes given in phi scale [$\phi \equiv -\log_2(\ell/\ell_0)$] shown on the plots.
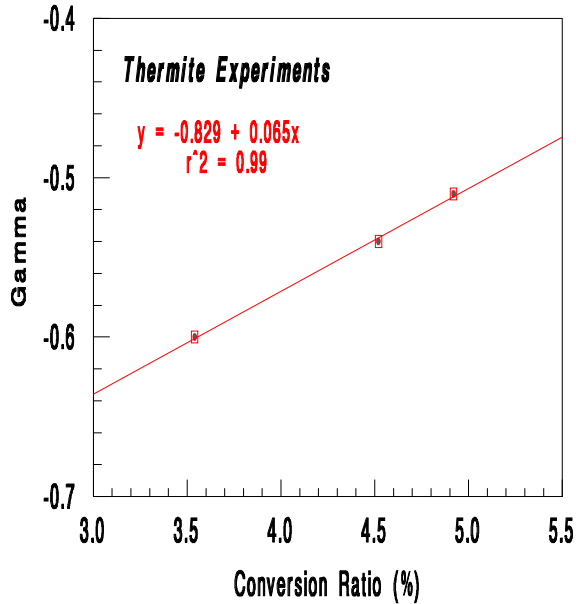

Figure 6. Plot of weighted average γ (gamma) value *vs* conversion ratio for experimental samples shown in Figure 5. For experiments involving little or no water with very low conversion ratios, gamma is expected to be less than -0.83.

Because we have so few experimental data to test the above hypothesis, we compare the experimental trends to data from the Neapolitan Yellow Tuff studied by Wohletz *et al.*[15] for which conversion ratios were constrained by calculated mechanical energies necessary to emplace the tephra. For these calculations, thermodynamic relationships based on adiabatic expansion of steam were used in the volcanic case, so the same conversion calculations were applied to the experimental data, which are somewhat higher than those calculated by measured mechanical energies shown in Figure 6. The plot of γ *vs* conversion ratio in Figure 7 shows a remarkable correlation in which γ increases linearly with conversion ratio. Magmatic samples (those having experience little or no fragmentation by contact with external water) are projected to have γ values near -0.9 while those hydrovolcanic samples resulting from energetic vapor explosions have γ values as high as -0.7. We note that the γ values for this set of data do not go as high as those from the experiments (Fig. 6), and we attribute this discrepancy to the unconstrained effects of tephra transport for which ballistic and traction flow cause an overprint of lower γ values. Still these results are compelling and suggestive for tests to be done on more controlled sets of data.

In further consideration of fragmentation mechanisms, Wohletz[14] showed experimental data and heat flux calculations suggesting that water/melt explosions showed increasingly finer grained ejecta debris with increasing explosivity. If the data shown in Figure 7 demonstrating increasing γ values with increasing conversion ratios (explosivity), then there should also be a similar increase in γ values with sample mode (which increases with decreasing average size on the phi scale). Indeed, this relationship is indicated by data both from the Neapolitan Yellow Tuff and tephra from the recent eruptions (1977) of the Ukinrek maar volcano[16] in Alaska (Figure 8). However, we note separate trends in the data for these two volcanoes, which bear out the fact that Ukinrek involved much more water-rich eruptions and smaller magma volumes (<<1 km^3) than did the Neapolitan Yellow Tuff (>35 km^3). The data in Figure 8 only show samples with modes finer than about 1 mm (0 ϕ), the empirical division by size between magmatic and hydrovolcanic fragmentation described by Wohletz.[14]

IV. Conclusions

Sequential fragmentation/transport theory (SFT) provides a method to predict fragment mass/size distributions for particulate samples derived from a variety of fragmentation and transport processes. Its derivation is based in physical laws and it allows incorporation of various solutions of the Navier-Stokes equations in determination of mass distributions. At this point, we have only a general idea of mass sensitivity involved in various fragmentation and transport processes, but we have data that support the application of SFT in order to learn more about fragmentation in water/melt explosions where debris samples can be obtained.
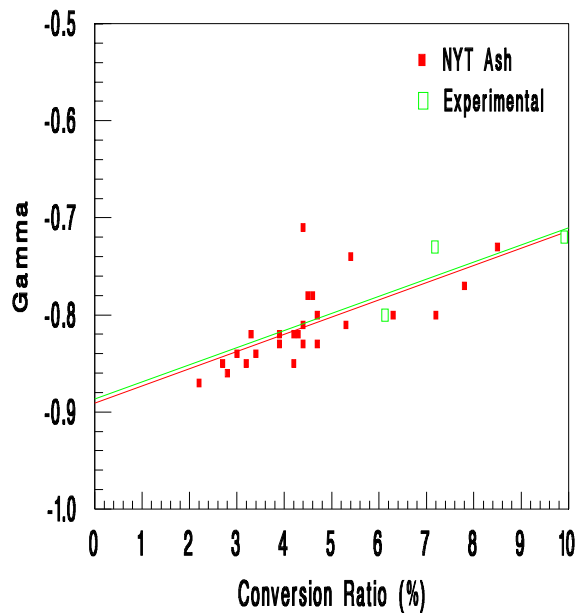
Figure 7. Plot of weighted average γ (gamma) value *vs* adiabatic conversion ratios for experimental and tephra (ash) samples from the Neapolitan Yellow Tuff.[15]
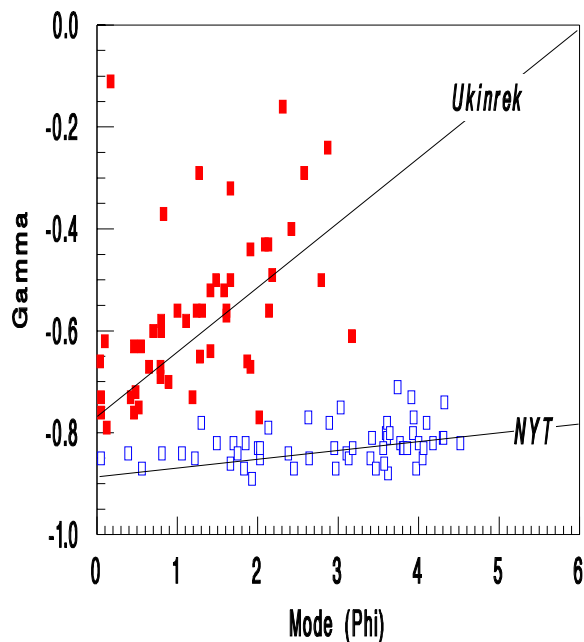

Figure 8. Plot of weighted average γ *vs* weighted average sample mode for samples from the Neapolitan Yellow Tuff (NYT) and Ukinrek maar volcano[16] define two distinct trends of increasing γ with mode.

The SFT free parameter γ describes the mass sensitivity of the given fragmentation processes, while for transport processes, the analogous free parameter is termed τ. It is this parameter that must be evaluated from theory to predict a distribution. The parameter varies from -1 (where a distribution is flat) to more positive values as fragmentation/transport processes require more repeated steps (*e.g.* repeated stressing and unloading events, repeated growth and detachment of instabilities, repeated transport and deposition of a fragment population). With increasing γ or τ, the distribution becomes finer and more peaked.

With the few experimental data we have analyzed, there appears to be an increase in sample size distribution γ values with an increase in vapor explosion thermal efficiency. This trend is also shown in samples of volcanic ash produced by hydrovolcanic eruptions for which γ values increase with increasing degree of external water interaction. We then conclude that intense multiphase vapor explosions involve various fragmentation/propagation mechanisms that depend on the mass ratio of water and melt interacting.

REFERENCES

1. D. E. Grady, "Fragmentation of solids under impulsive stress loading," *J. Geophys. Res.*, **86**, 1047-1054 (1981).

2. W. K. Brown, "A theory of sequential fragmentation and its astronomical applications," *J. Astrophys. Astr.* **10**, 89 (1989).

3. W. K. Brown and K. H. Wohletz, "Derivation of the Weibull distribution based on physical principles and its connection to the Rosin-Rammler and lognormal distributions," *J. Applied Phys.*, (in press), (1995).

4. W. Weibull, "A statistical theory of the strength of materials," *The Royal Swedish Institute of Engineering Research*, Proc. No. **151**, Stockholm (1939).

5. B. B. Mandelbrot, *The fractal geometry of nature*, W. H. Freeman and Co., New York (1983).

6. P. Rosin and E. Rammler, "The laws governing the fineness of powdered coal," *J. Inst. Fuel*, **7**, 29-36 (1933).

7. K. H. Wohletz, M. F. Sheridan, and W. K. Brown, "Particle size distribution and the sequential fragmentation/transport theory applied to volcanic ash," *J. Geophys. Res., **94**, 15,703-15,721 (1989).

8. L. G. Austin, "Size reduction of solids: Crushing and grinding equipment," *Handbook of Powder Science*

and Technology, 562-606, Van Nostrand Reinhold, New York (1984).

9. D. McAlister, "The law of the geometric mean," *Proc. Roy. Soc. London*, **29**, 367-376 (1879).

10. A. I. Medalia and F. A. Heckman, "Morphology of aggregates-II. Size and shape factors of carbon black aggregates from electron microscopy," *Carbon*, **7**, 567 (1969).

11. K. H. Wohletz and R. G. McQueen, "Experimental studies of hydromagmatic volcanism," *Explosive Volcanism: Inception, Evolution, and Hazards*, edited by F. R. Boyd, Jr., pp. 158-169, Studies in Geophysics, National Academy Press, Washington, D. C. (1984).

12. K. H. Wohletz, "Experimental study of hydrovolcanism by fuel-coolant interaction analogs," this volume, (1995).

13. G. Heiken and K. Wohletz, *Volcanic Ash*, University of California Press, Berkeley, California, 246 p. (1985).

14. K. H. Wohletz, "Mechanisms of hydrovolcanic pyroclast formation: grain size, scanning electron microscopy, and experimental results," *J. Volcan. Geotherm. Res.,* **17**, 31-63 (1983).

15. K. H. Wohletz, G. Orsi, and S. de Vita, "Eruptive mechanisms of the Neapolitan Yellow Tuff interpreted from stratigraphic, chemical, and granulometric data," *J. Volcan. Geotherm. Res.*, (in press) (1995).

16. M. H. Ort, K. H. Wohletz, and C. A. Neal, "Complex interaction of ground water and basaltic magma during the eruption of the Ukinrek maars, Alaska," *Geol. Soc. Amer. Abs. with Prog.*, **26(7)**, A378 (1994).